FORM C
COLLEGE SCHOLARS PROJECT APPROVAL

Elizabeth Jacobs
Scholar

Fred M. Schaeffer
Mentor

Structural and Magnetochemical Studies of Ag^{II} in Fluoride Lattices with Emphasis on Cs_2AgF_4
Project Title

COMMITTEE MEMBERS
(Minimum 3 Required)

Name	Signature
Fred M Schaeffer	
Jan Masfeldt	
Claudia Rewn	

PLEASE ATTACH A COPY OF THE SENIOR PROJECT TO THIS SHEET AND RETURN BOTH TO THE PROGRAM DIRECTOR. THIS PAGE SHOULD BE DATED AND COMPLETED ON THE DATE THAT YOUR DEFENSE IS HELD.

DATE COMPLETED Nov. 13, 2009

Structural and Magnetochemical Studies of Ag^{II} in Fluoride Lattices with Emphasis on Cs_2AgF_4

Elizabeth A. Jacobs

November 4, 2009

Contents

List of Figures

List of Tables

Chapter 1

Introduction

All materials are magnetic, due to the presence of electrons surrounding the atoms that interact and bind to make each compound. Electrons are fermions, sub-atomic particles with a spin of $\frac{1}{2}$. The electrons in a material reside in and fill orbitals belonging to each atom, and as they do so the electrons will naturally spin pair. This pairing of spins is described by Hund's Rule and the Pauli Exclusion Principle, which summarizes the behaviors of electrons in an atom by stating that no two electrons can be described by the exact same quantum numbers. Due to this spin pairing, and since all materials contain a core of spin paired electrons, all materials have inherent *diamagnetism*. A scheme of the diamagnetic spin arrangement is give in Figure 1.1 below.

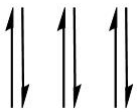

Figure 1.1: Diamagnetic spin arrangement

A pure diamagnet contains an even number of electrons that naturally reside in a ground state which has *only* spin pairing. In other words, the overall spin of the system is zero

since each electron with a spin of $+\frac{1}{2}$ pairs with an electron with a spin of $-\frac{1}{2}$. Two examples of well recognized materials which are characterized diamagnets include ammonia[4] and methane.[4] Although all materials have inherent diamagnetism, due to paired core electrons, not all materials are *pure* diamagnets. One must also consider the behavior and arrangement of the valence, or outermost electrons. The valence electrons are most often of more interest than the core electrons (due to the different magnetic arrangements which they may adopt), and are in part responsible for the behavior of a molecule. Some materials contain atoms which have one or more unpaired valence electrons in addition to their paired core electrons. These unpaired valence electrons on the individual atoms will couple with each other, which produces measurable magnetic properties in the material.

Materials with *unpaired valence* electrons are called *magnetic materials*. In order to investigate these magnetic materials, an external magnetic field is commonly applied to the material. When a magnetic field is applied, the unpaired electrons in a magnetic material are likely to produce a spin arrangement that is present throughout the bulk of the material. Four common forms of spin arrangement are possible, depending on the electronic environment and orbital description of the material. These are *paramagnetism*, *ferromagnetism*, *antiferromagnetism* and *ferrimagnetism*. These magnetic arrangements are reflected in the value of the coupling constant measured for each environment. This value measures the amount of coupling which occurs with the magnetic interaction. The coupling constant is represented as J, and the magnitude of J with respect to each form of magnetism is give in Table 1.1.

The magnetochemistry of a material reflects the arrangements of the electron spins in response to an applied magnetic field and is therefore related to the electronic properties of the material. A strong correlation exists between the electronic and magnetic properties of a material and therefore with its physical properties as well. One property of magnetic materials

Table 1.1: Forms of magnetism and corresponding value of J

Magnetic form	J value
Paramagnetism	0
Antiferromagnetism	< 0
Ferromagnetism	> 0
Ferrimagnetism	< 0

which is of current interest is the extent of each material's ability to conduct electricity, or how well it is able to inhibit this conduction. Certain materials will conduct electricity with a specific percent efficiency, which varies with the material composition, and some materials do not conduct at all. These materials may be classified as either conductors (semi-conductors) or insulators, depending on the extent to which they are able to conduct electricity. However, perhaps one of the most desirable and scientifically interesting properties observed in materials is the ability to *superconduct*. A superconducting material is able to transport an applied electrical current with *zero* resistivity. Superconductors could be highly efficient and potentially a material of choice to make items such as computer chips, mobile phone components and wires used for long distance connections. At present, all known superconducting materials will only display this phenomenon at very low temperatures (well below the freezing point of water), making them poor choices for practical applications. In addition, the general mechanism by which these materials are able to conduct with zero resistance is unclear. Given that there is no clear general mechanism and that the phenomenon is only present at low temperatures, exploratory synthesis is important in order to discover materials which display new magnetic arrangements in the solid state.

Within the past decade, a few superconducting systems have gained attention with promising information regarding the essential characteristics for superconductivity as well as their ability to superconduct at higher temperatures than ever before. Much work has been reported on the parent phase La_2CuO_4 and its superconducting doped phases of various compositions, specifically $La_{2-x}M_xCuO_4$ with M = Ba,[5] Sr[6,7] and Ca[8] and $x = 0.1, 0.2$. It is suspected that the conditions which are required for superconductivity are supplied to this system by the $3d^9$ Cu^{II} center because it is the source of the magnetic properties of the material, and that chemical doping with non-magnetic ions encourages the emergence of a superconducting phase. It seems fitting, then, to partake in exploratory synthesis to prepare systems with apparent structural and electronic similarities to the layered copper oxide La_2CuO_4. The studies reported herein describe investigations of the Ag^{II} ion (heavier analogue of the Cu^{II} ion) parent ternary silver fluoride Cs_2AgF_4 and its barium doped phases. Cs_2AgF_4 is known to be structurally similar to the parent copper oxide La_2CuO_4[9] but has different magnetic properties and lacks the formation of superconducting phases when doped. This exploratory synthesis provides steps towards the discovery of new magnetic materials as well as defining a set of properties required for superconductivity. Moreover, these new materials will help to refine our understanding of the general mechanism for superconductivity through direct comparison with known superconductors.

Chapter 2

Background and theory

2.1 Chemistry of Ag^{II} in fluoride lattices

Divalent silver is a unique species which has been closely investigated by both theoreticians[1] and experimentalists.[10] In comparison to the other known oxidation states of silver, Ag^{I} and Ag^{III}, the Ag^{II} ion is rare. When exposed to trace amounts of water in the atmosphere, species which contain Ag^{II} will react chemically with the water molecules to produce an array of species which contain Ag^{I}, or a disproportionation product containing a [Ag^{I}-Ag^{III}] network. This strong interaction with very small amounts of atmospheric moisture, even as low as a parts per million concentration, provides reference to the very strong oxidizing power[11] of Ag^{II}. The Ag^{II} ion is such a strong oxidant that it will spontaneously oxidize the oxygen in water to gaseous elemental oxygen via the following reaction:

$$2\,Ag^{2+} + H_2O \longrightarrow O_2 + 2\,Ag^{+} + 2\,H^{+}$$

Due to this tendency, species which contain the Ag^{II} ion must be handled in an inert atmosphere, such as nitrogen or argon, or in anhydrous hydrofluoric acid (aHF). In these environ-

ments, the Ag^{II} ion is stable, but is still often used as an oxidant. One notable instance was published by Neil Bartlett.[12] He reports using a carefully controlled aHF reaction medium. He was able to oxidize the noble gas xenon, Xe^{0}, to Xe^{II} with the Ag^{II} ion to create the stable noble gas containing compound XeF_2.

Many systems which, at first glance, appear to contain Ag^{II} in fact contain silver atoms in various and mixed oxidation states. This most commonly consists of a network of Ag^{I} and Ag^{III} ions forming a mixed oxidation state [Ag^{I}-Ag^{III}] species.[13,14] For example, the compound AgO was once thought to contain one true Ag^{2+} ion for every O^{2-} anionic species in the lattice.[15] However, experiment proves that this species should correctly be thought of as [Ag^{I}-$Ag^{III}O_2$], Ag_2O_2. This result is confirmed through magnetic measurements,[16] which report that AgO is a diamagnet. This diamagnetism implies that there are no unpaired electrons in this system, thus eliminating the oxidation state assignment of the silver as $2+$, since the $4d^9$ valency of Ag^{2+} would contain unpaired electrons.

Despite the reactivity of Ag^{II}, compounds which contain true Ag^{II} exist and usually have interesting properties or reactivity characteristics. The Ag^{II} ion has a $4d^9$ valence electronic configuration, which is in part responsible for the unique nature of these species. However, because of the $4d^9$ valence electron configuration, the Ag^{II} ion, when in a ligand field, is subject to strong Jahn-Teller distortions.[10] The Jahn-Teller effect occurs due to the presence of degenerate orbitals in the ground state of a molecule. This degeneracy causes instability in the species' ground state and, in response, the species will adopt a lower geometry, in order to remove this degeneracy. The lower geometry occurs in the form of characteristic distortions to the ground state geometry.[17] The distortions are observed as elongation or shortening of two of the six bonds in the octahedron in order to lower the total energy of the system. In most cases, the octahedral geometry will adopt a lower energy D_{4h} environment. This geometry

is seen in the [AgF_6^{4-}] distorted octahedrons in the ternary silver fluoride Cs_2AgF_4. This feature produces the interesting magnetic properties of the material.[18]

2.2 Magnetism and superconductivity

While all materials have inherent diamagnetism, those which contain unpaired electrons display one of four competing forms of magnetism which makes them particularly interesting. In almost every case, the competing form of magnetism displayed by a material has such a significant effect on the material's properties that it overwhelms the inherent core diamagnetism under experimental conditions and is predominantly observed in measurements. In addition, the measured magnetism produces unique properties displayed by the material. These properties are often highly desirable and may be used in practical applications, such as computer chips and mobile phones. Therefore, materials which display these properties are closely investigated by research scientists across the globe. The four forms of magnetism which arise from the presence of unpaired electrons of a material, often in response to the presence of an applied magnetic field, have been mentioned and are described further below. A pictorial representation accompanies each of the following descriptions.

Paramagnetism is described as a random and non-ordered arrangement of unpaired electrons in a material. A unique aspect of paramagnetism is that, along with diamagnetism, it is not dependent on the presence of a magnetic field, and paramagnetism is observed in compounds under ambient conditions. Most materials at room temperature are either characterized as diamagnets or paramagnets.

Ferromagnetism occurs when, in response to the application of an external magnetic field, spins from neighboring atoms arrange in what is described as a 'spin-up, spin-up' fashion.

Figure 2.1: Paramagnetic spin arrangement

In other words, all spins are oriented in the exact same upward direction as those above, below or next to them creating a bulk arrangement of uniform magnitude. A well known ferromagnet is elemental iron, with the term *ferro*magnet originating from the observed spin response from an iron sample.

Figure 2.2: Ferromagnetic spin arrangement

Antiferromagnetism is the electronic arrangement opposite to that of ferromagnetism, in that unpaired electrons arrange in a 'spin-up, spin-down' fashion in relation to one another. This creates a bulk electronic structure of planes with alternating spin orientations, but with the magnetic moment of the spin-up and spin-down being equal in magnitude.

Figure 2.3: Antiferromagnetic spin arrangement

Ferrimagnetism is a form of electronic arrangement similar to that of antiferromagnetism but with spins of opposite direction having different magnitudes. This form of magnetism is not as relevant to the present study of the silver fluoride system of interest and will not be discussed in further detail.

Figure 2.4: Ferrimagnetic spin arrangement

Magnetic materials that display bulk electron spin arrangements throughout their lattice often provide an environment which will support and facilitate unique properties, specifically the ability to conduct electricity or function as an insulator. Numerous reports in the literature describe materials which will not conduct electricity (insulators) or will only conduct electricity at a certain efficiency (semiconductors). However, a growing number of very unique compounds have been reported which are able to transport an applied electrical current with complete efficiency. These materials are called *superconductors*, and their discovery in 1911 has prompted new and focused areas of research in chemistry, physics and materials sciences. Table 2.1 provides some examples of magnetic materials and their critical temperatures, below which their magnetic phases are present and they display bulk properties including the ability to superconduct.

Table 2.1: Materials and their critical temperatures

Material	Critical temperature (K)	Material	Critical temperature (K)
Tl[19]	2.384	$NbSe_2Mn_{0.33}$[20]	22
Sn[19]	3.728	$La_{1.8}Sr_{0.2}CuO_4$[21]	36
In[19]	3.404	$NbSe_2Cr_{0.25}$[20]	79
Hg[19]	4.153	$Y_{0.33}Ba_{0.67}CuO_{2.33\pm\delta}$[22]	87
Ta[19]	4.304	$Hg_{0.8}Tl_{0.2}Ba_2Ca_2Cu_3O_{8+\delta}$[23]	138

Today there are two generally accepted theories of superconductivity, one for systems which display superconductivity at lower temperatures and another for those which superconduct at higher temperatures. The low temperature theory, which was originally thought to be the definitive theory of superconductivity, was first described by a team comprised of J. Bardeen, L.N. Cooper and J.R. Schrieffer and is today known as the BCS theory of superconductivity.[24] This theory describes the formation of *Cooper pairs*, pairs of electrons, which travel through the crystal lattice with zero resistance. The electrons are propelled through the lattice by lattice vibrations,[25] called phonons. While these vibrations are present in all states of matter, at very low temperatures the vibrations in solids can be small enough to not disrupt travel of these electron pairs but rather facilitate their travel. This theory was once used to predict the maximum temperature at which superconductivity will occur in all superconducting materials. However, with the discovery of materials which superconduct above this temperature, and currently with discoveries of materials which superconduct well above this temperature, a new theory is needed to describe superconductivity in new materials.

This new theory, the theory of high temperature superconductivity, attempts to account for all of the conditions in the BCS theory for which the high-temperature superconductors do not maintain. Instead of a proposed cooper pair formation through which electrons may travel, the high-temperature theory suggests that specific essential orbital interactions, called super exchange, must occur between the magnetic metal center and the counter ions. The high-temperature superconductors in a way are more exciting and relevant to current searches, simply because they display the desired phenomena and temperatures close to those which are applicable in technology and society. One such material in particular is the lanthanum copper oxide La_2CuO_4. This species, when doped, yields materials which display superconducting phases at low temperatures and has led to the investigation of numerous copper-oxides.

2.3 Literature review

Since the discovery of superconductivity in elemental mercury, scientists have pursued the synthesis of materials with increasingly high critical temperatures for purposes such as implementing these materials in computers, mobile phones and other constantly developing forms of technology. Efforts with these materials go towards the hope of one day finding a material which is able to superconduct at room temperature. Those materials which were investigated in the early days of superconductivity are now referred to as low-temperature superconductors. Over the past 100 years, the discovery of materials which are able to superconduct at much higher temperatures than the 4.153 K transition temperature of mercury[19] have prompted the formation of a *second* theory of superconductivity, one which seeks to describe the mechanism by which this phenomenon occurs. This high-temperature superconductivity and the materials which display superconductivity at higher temperatures than those predicted by the BCS theory has led to a handful of fundamental advancements in this area of study.

Of particular interest is the rise of the class of copper-oxide high-temperature superconductors. This began in 1986, with the discovery of the first high-temperature superconductor, a $\mathrm{Ba-La-Cu-O}$ system.[26] It's critical temperature, 35 K, was higher than the maximum critical temperature predicted by the BCS theory of superconductivity (30 K). The authors, Bednorz and Muller shared the 1987 Nobel prize in physics for their discovery. Shortly after the report of this compound, a search ensued to find materials with increasingly higher critical temperatures. Following the $\mathrm{Ba-La-Cu-O}$ system, a $\mathrm{La-Sr-Cu-O}$ compound was reported with a critical temperature close to 40 K,[27] and within months systems of $\mathrm{Y-Ba-Cu-O}$ with critical temperatures around 90 K topped the temperature scale. An-

other important breakthrough came when the first material with a critical temperature over 100 K was reported. This was the copper oxide $Bi_2Sr_2Ca_2Cu_3O_{10}$, and it has a measured critical temperature of 114 K.[28] Currently, the material holding the current record for highest reported critical temperature is the thallium doped copper oxide, $Hg_{0.8}Tl_{0.2}Ba_2Ca_2Cu_3O_{8+\delta}$ with a critical temperature of 138 K.[23]

Due to the magnitude of impact of the copper oxide phases, a comparison between copper oxide and silver fluoride interactions has been brought into consideration. A 2001 review of silver fluorides by Hoffman and Grochala[1] took its audience through almost every characterized silver fluoride species, explaining the theoretical aspects behind a potential silver fluoride superconductor. In 2006, Grochala followed up his review with a report which compared and contrasted the electronic structure for $Cu-O$ and $Ag-F$ motifs.[29] Results from this paper showed that 'charged doped silver fluorides had good prospect for superconductivity.' Up until then, most of the synthetic work on silver fluorides had been reported by Neil Bartlett,[12,30–33] B. G. Muller[34–40] and Boris Zemva.[12,30,31,40–43] Of the compounds studied, the ternary silver fluoride Cs_2AgF_4 is most structurally similar to the ternary copper oxide La_2CuO_4. Charge doping studies on Cs_2AgF_4 which mimic those of La_2CuO_4 would provide confirmation or argument towards the theoretical outcomes reported by Grochala. Preliminary results (unpublished) from Dolgos and Turner regarding the project reported herein describe an increase in the critical temperature of Cs_2AgF_4 with minimal charge doping. A continuation of these studies is presented in the following chapters.

Chapter 3

Methods of Analysis

3.1 Magnetic measurements of Cs_2AgF_4

Magnetic materials, due to their bulk spin arrangement, have a very detailed electronic structure. This structure is directly responsible for the observed properties. While current emphasis in characterization research is focused on utilizing neutrons to probe materials (elastic and inelastic neutron scattering), neutrons are not suitable probes for the materials studied herein. This is because the silver atoms in Cs_2AgF_4 and the barium doped derivatives of Cs_2AgF_4 tend to absorb the neutrons and turn over inconclusive characterization data. Muons, on the other hand, are very ideal particles to use in this type of experiment. A muon is an elementary particle which will act as a microscopic probe for magnetic materials. Their small size allows them to reside within a crystal lattice and adopt the bulk spin orientation. In addition, and in particular with the species involved, the muon may participate in the formation of a $[F-\mu-F]^-$ species,[44] which is directly detectable with current instrumental standards. The muon will implant into the lattice of the Cs_2AgF_4 sample and form a 'hydrogen bonded ($[F-\mu-F]^-$) ion, which will cause a distinct muon relaxation signal.'[44] These species were

detected in the reported experiments and play a role in determining the local magnetic environment on each plane of the lattice.

In a muon spin resonance (or muon spin relaxation or rotation) experiment, spin polarized muons are produced on a synchrotron ring and are implanted into the sample of interest. A beam spin of polarized muons is produced when all of the muons adopt the same spin arrangement. At ISIS, the muon beam is completely polarized. Once stopped in the sample, the muon will occupy an interstitial site within the crystal lattice and then adapt to the local spin arrangement, due to the influence of the material's magnetic properties. A muon is able to behave in this way because, like the electrons which compose the magnetic environment, a muon is a fermion and has non-integral spin. Fermions are subatomic particles which have a spin of one-half. The muon's spin will behave in such a way that it will mimic the local spin structure of the sample while it is occupying a place in the lattice during its lifetime ($2.2\ \mu s$). At the end of its lifetime, the muon will decay into a positron. Positron detectors positioned around the sample in the instrumental setup detect the positrons emitted from the sample and from the direction in which they arrived at the detector are able to produce a picture of how the muons were arranged within the lattice.

3.2 The muon spin resonance experiment at ISIS

Currently, there are four facilities across the globe which are able to produce spin polarized muons. The MuSR instrument at ISIS (Didcot, UK) was used to measure a polycrystalline sample of Cs_2AgF_4. All muon resonance experiments begin at an ion source. At ISIS, this ion source is a chamber which consists of hydrogen (H_2) gas and hot cesium vapor (the boiling point of cesium is 978 K).[45] The reaction between the gaseous hydrogen and the cesium vapor

forms a discharge plasma, which consists of charged particles (Cs^+ and H^-, the hydride ion). These ions are separated by a cathode, which attracts the positive Cs^+ ions and leaves only the hydride ions in the ionization chamber. These hydride ions are then extracted from the ion source in 200 μs pulses (in other words, a fraction of the hydride ions which have been produced in the ionization chamber are removed in a batch every 200 μs or $2\text{x}10^{-4}$ s). These pulses are narrowed and eventually turned into a beam of hydride ions, which are then sent through a magnet which bends the beam 90° from its initial path. The function of this magnet, and the abrupt change in beam pathway, is to strip the beam of any residual electrons which are bunched with the hydride ions in the ionization chamber. The hydride ions are then passed over an acceleration gap, which produces a beam energy of 35 KeV. With residual electrons removed and a constant energy of 35 KeV, the hydride beam is re-focused and transported through the low energy beam transport. The low energy beam transport brings the hydride beam through another accelerator, the radio frequency quadrupole accelerator. The radio frequency quadrupole accelerator applies electrical fields to the beam, and these fields are carefully oriented in such a way that they are able to focus, bunch and accelerate the hydride beam. From here, discrete bunches of hydride ions which are extracted at 4.94 ns intervals are passed on to the linear accelerator (linac). In the linac, the hydride beam is accelerated to 70 MeV, and pulses are extracted every 200 μs to travel to the synchrotron ring.

The synchrotron ring at ISIS has a 26 m radius, giving it a circumference of approximately 163 m (534 ft). The ring is equipped with 10 dipole magnets, which maintain the alignment and intensity of the beam. In the synchrotron, the hydride ions which make up the beam are stripped of their electrons, turning them into protons.

$$H^- \longrightarrow H^+ + 2\,e^-$$

The protons will continue in the synchrotron ring until they complete approximately 130 revolutions. During these revolutions, a radio-frequency system will separate the proton beam into two equal halves. These halves travel at the same time in the synchrotron ring as they are accelerated to 800 MeV, and a constant proton beam orbit is maintained. These beams make $10,000$ revolutions in the synchrotron ring and then are put into a single revolution. In batches of protons, these beams are sent to the neutron and muon targets. The entire process, from ion source to final transport to the neutron and muon targets occurs roughly 50 times per second.

At ISIS, the proton beam will collide with a tungsten target to produce mostly neutrons for elastic and inelastic neutron scattering experiments. However, some of the beam will then collide with a muon target to start the production of muons for muon spin resonance experiments. The muon target at ISIS is a 10 mm thick carbon (graphite) block. Upon proton collision with the carbon block, a beam of pions is produced. The pion is an elementary particle which is one of the decay products of the muons within the sample. These pions have a lifetime of roughly $2.6\text{x}10^{-8}$ seconds, after which time they will decay into muons. The muons are then implanted directly into the lattice of a sample as local magnetic probes. Once in the sample, muons have a lifespan of 2.2 μs ($2.2\text{x}10^{-6}$ seconds), at which time they will decay into positrons. The muon spin resonance instrument at ISIS is equipped with a positron detector, which serves to measure the characteristics of the positron decay particles emitted from the sample. With these characteristics, computing software can infer the local muon environment in the sample of interest.

The table below summarizes the important features of the MuSR instrument at ISIS, which is one of three muon spectrometers (the others being Hifi and Emu). The MuSR instrument is the ideal instrument at ISIS to measure magnetism and superconductivity char-

acteristics of solid state materials.

Table 3.1: Instrument parameters for MuSR at ISIS

Number of detectors	Measurements	Field	Temperature
64	Longitudal and transverse	Maximum 2500 G	40 mK - 1000 K

3.3 Structure measurements of Cs_2AgF_4 derivatives

The diffraction of X-rays by single crystals was first observed by Sir William Henry Bragg and Sir William Lawrence Bragg, a father and son team, who later shared the Nobel Prize (1915, Physics) for their work towards detailed understanding of the diffraction phenomenon. Shortly after, the fundamental mechanism by which X-rays are diffracted by a crystal lattice was mathematically proven and explained via Bragg's Law of diffraction, formulated by W.L. Bragg in combination with his father's work. Alongside the physical mechanism and mathematical treatment of X-ray diffraction, advances in instrument configuration and X-ray intensity have allowed scientists to employ diffraction and similar techniques in order to study the structure (and thus properties) of many types of systems. Since the time of these initial discoveries and proofs, investigations with X-ray diffraction techniques, either using a single crystal or powder sample, has become a popular means of structural characterization.

Crystalline (powder) materials display bulk atomic arrangement usually presenting in the form of repeating units called the unit cell. Due to the fact that these samples are not single crystals but rather a collection of near-perfect crystallites, the orientation of these unit cells are random in nature and may contain faults. Because of this (near) perfect arrangement and

packing, a 'diffraction gradient' is formed which may be used as a surface upon which a directed X-ray beam may be diffracted. When placed in the path of such light, the electron density surrounding each atom provides an interaction site for the incident X-ray, causing diffraction. The angle of this change is considered in analysis of the diffraction experiment in order to extract relevant crystal data. This is accomplished through the use of Bragg's Law:

$$n\lambda = 2dsin(\theta)$$

Bragg's Law takes into account the wave nature of light and where n is the order of diffraction (which takes the form of an integer and is usually assumed to be 1), d is the interatomic distance, commonly referred to as the d-spacing and θ is the angle of diffraction. In a uniformally crystalline solid, the use of Bragg's Law to calculate peak position in a diffraction pattern. Bragg's Law represents the relationship between the diffracted X-rays and peak positions in the diffraction pattern as a series of incident angles of diffraction and interatomic distances repeating uniformally within the crystal structure. From this, a crystal structure can be simulated and the bond lengths and angles of the species quantified.

In instances when a single crystal is unobtainable, a finely ground powder will suffice as a diffraction gradient. In contrast to a single crystal, where all atoms are arranged in the lattice in one fixed orientation, a powder sample is composed of small crystalline units which rest in every possible orientation. Due to the random nature of these orientations it is necessary expose a large number of crystallites to the incident X-rays. This is sometimes accomplished by containing the sample in a small diameter capillary tube. During the experiment, the capillary is mounted and rotated continuously in such a way that the incoming X-ray beam may diffract off of each random orientation, providing a complete representation of the unit cell in the data received. The capillary mount geometry is called Debye-Scherrer.

3.4 The diffraction Experiment at NSLS

The National Synchrotron Light Source (NSLS) is part of Brookhaven National Laboratory (BNL), located in Upton, New York. The National Synchrotron Light Source facility is a special division of BNL which operates an electron synchrotron for the study of materials. Specifically for the samples measured and presented herein, this electron beam is a source of variable energy, and thus wavelength via $E = h/c\upsilon$, X-rays to study the atomic structure of single crystal or powder samples.

At NSLS, the synchrotron ring is charged with electrons in the form of an electron beam. These electrons travel around the circumference of the ring in *bunches*, similar to the *pulses* in which protons travel at ISIS. During their travel, the beam is maintained and guided by very strong magnets which focus the beam and provide a well defined path along which the electrons travel. As the electrons experience acceleration as they travel through the ring, they give off energy in the form of light. This is known as *synchrotron light*, and it ranges in wavelength from high-energy X-rays to the longer wavelengths of ultra violet, visible and infra red light. The synchrotron light in a relevant wavelength range is supplied to each instrument. Once directed to a specific instrument, the setup of the instrument will refine and focus the beam for the specific type of measurement necessary.

The X14A beamline leads to a capillary mount powder diffractometer. X14A is equipped with a mirror close to the entry point of the beam, which is used to redirect the beam into the instrument's monochromator. The monochromator serves to select the appropriate beam wavelength. Once through the monochromator, the beam will travel through a liquid helium chiller and is then passed through a slit which once again focuses the beam so that it will interact directly with the sample.

Each powder sample was mounted on the diffractometer and rotated about the long axis of the capillary throughout the course of the experiment. Once beam diffraction occurs upon interaction with the atomic lattice of the sample, the diffracted X-rays are directed through a second slit to a Ge^{III} crystal analyzer and then to the detector. X-ray intensity is recorded as a function of the angle 2θ. Table 3.4 provides a few of the instruments operational parameters.

Table 3.2: Instrument parameters for X14A at NSLS-BNL

Energy (KeV)	Wavelength ($\AA$)	Crystal Analyzers
5-26	0.477-2.479	Ge^{III}, LiF, graphite

Data was collected with an X-ray wavelength of $0.7736\AA$ (16 KeV) and a step size of 0.003 degrees θ from 2θ range of 5.5°and 59.5°. Diffraction from each sample was recorded for approximately 12 hours with the sample held at room temperature. The diffraction data was analyzed using the General Structure Analysis Program (GSAS).[46]

In the GSAS program, the Rietveld refinement method[47] is used to analyze and correct the collected diffraction data to fit the pattern of a known crystallographic model. This is accomplished through the adjustment of profile parameter to fit the peak shape (Lorentzian peak shapes are typical for synchrotron data), background and unit cell to produce the fully refined powder diffraction data set. Each collected powder pattern file was fit to the reported diffraction pattern and structural characteristics of the parent compound Cs_2AgF_4 published by McLain *et. al.*[9]. This piece of literature reports the correct space group of Cs_2AgF_4, *Bbcm*, as opposed to the previously reported and accepted space group (*I*4/*mmm*).

Chapter 4

Results and discussion

Almost 100 years after its discovery, the phenomenon of superconductivity is still not clearly understood. Since the 1911 report by Onnes of the first observation of superconductivity in elemental mercury, numerous other phases have been reported as both low temperature and high temperature superconductors. Some very notable examples of both low temperature and high temperature superconducting elements and phases are given in Table 1.1. At present, much attention is paid to the lanthanum copper oxide phase La_2CuO_4, which is the precursor to superconducting phases of various chemical dopant stoichiometries. The Cu^{II} ion found in La_2CuO_4 has a strong influence on the superconducting properties observed in these systems. For this reason, experimental and theoretical studies of La_2CuO_4 have been carried out in order to accurately describe the electronic and magnetochemical environments produced by these Cu^{II} ions which promote a chemical environment that supports this phenomenon. A creative way to identify properties which are necessary to support superconductivity is to synthesize systems with very similar electronic and magnetochemical descriptions of known superconductors and compare and contrast those of the new systems with known systems in order to deduce a list of characteristics which favor the formation of superconducting states.

A natural extension to the study of La_2CuO_4 would be to synthesize a phase which displays $[AgO_2]$ layers analogous to the $[CuO_2]$ layers found in La_2CuO_4 in which superconductivity occurs. Since a system which contains the $[AgO_2]$ motif is likely to possess a Ag^{II} ion, it would be convenient to compare the effects of this ion versus the Cu^{II} ion found in La_2CuO_4. However, to our knowledge there are no known systems to date which display such chemical architecture.[9] A structurally similar system, which contains the Ag^{II} ion is the ternary silver fluoride Cs_2AgF_4. This phase is of current interest due to its structurally similar crystal lattice as La_2CuO_4, with the only noticeable difference being the angles at which the $[AgF_6]$ octahedra align with respect to one another in relation to the arrangement of $[CuO_6]$ octahedra in La_2CuO_4.

The structure of Cs_2AgF_4 is well defined and understood. The crystalline lattice is built from alternating $[AgF_2]$ and [CsF] layers in an $[AgF_2]$[CsF][CsF]$[AgF_2]$ layer stacking scheme as is seen in the figure below:

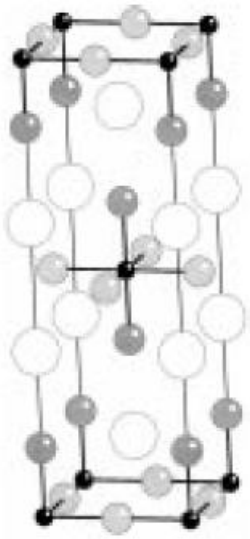

Figure 4.1: *Crystal structure of Cs_2AgF_4*[1]

In the above figure, the black atoms are silver, the grey are fluorine and the white are

cesium. Within these layers, $[AgF_6]^{2-}$ octahedra are formed, with the axial F−Ag−F of each octahedron being perpendicular to the neighboring $[AgF_6]^{2-}$ octahedra. Such an arrangement, with neighboring octahedra being perpendicular to one other, is known as an antiferrodistortive arrangement. This is directly responsible for the ferromagnetism observed in these material below 13.95 K, as an antiferrodistortive lattice arrangement will typically lead to ferromagnetism when the material is cooled to or below its critical temperature. Despite the similar layering scheme found in Cs_2AgF_4 and La_2CuO_4 ([CsF] and [AgF_2] layers analogous to [LaO] and [CuO_2] layers), a distinct difference in their crystal structures are the orientation of the $[AgF_6]^{2-}$ and $[CuO_6]^{2-}$ octahedra (respectively) arranged within the crystal lattices with respect to neighboring octahedra. In Cs_2AgF_4, the octahedra arrange so that the Ag^{II} ions form an antiferrodistortive magnetic arrangement, leading to bulk ferromagnetism in the doped variants at their critical temperature. However, in La_2CuO_4, the magnetic arrangement of Cu^{II} ions is ferrodistortive, leading to bulk antiferromagnetism in doped samples below the critical temperature. In contrast to the previously described antiferrodistortive arrangement, a ferrodistortive arrangement is described by a parallel alignment of the elongated axes of neighboring octahedra. The structural differences between Cs_2AgF_4 and La_2CuO_4 can be interpreted more descriptively in the image in Figure 4.2 published by Grochala in the July 2006 volume of *Nature Materials*. As can be clearly identified, the $[AgF_6]^{2-}$ octahedra in Cs_2AgF_4 arrange so that their elongated F−Ag−F axes are perpendicular to each other (antiferrodistortive arrangement) and in contrast, the $[CuO_6]^{2-}$ of La_2CuO_4 are arranged in a parallel fashion (ferrodistortive arrangment).

The structural and magnetochemical studies of Cs_2AgF_4 and a few of its doped derivatives are described herein. Muon spin resonance experiments were carried out at ISIS in the UK and X-ray diffraction experiments were carried out at the NSLS in Upton, New York.

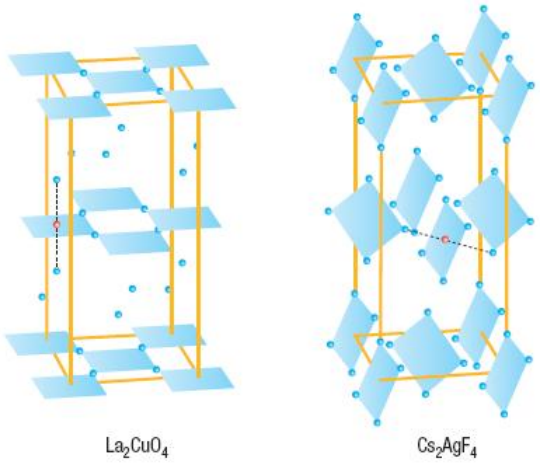

Figure 4.2: *Crystal structures of Cs_2AgF_4 and La_2CuO_4*[2]

4.1 Discussion of the magnetic measurements of Cs_2AgF_4

A polycrystalline sample of the parent compound Cs_2AgF_4 was synthesized and its magneto-chemical properties assessed using muon spin resonance techniques. A full plot of the spectra obtained from this measurement is given below.

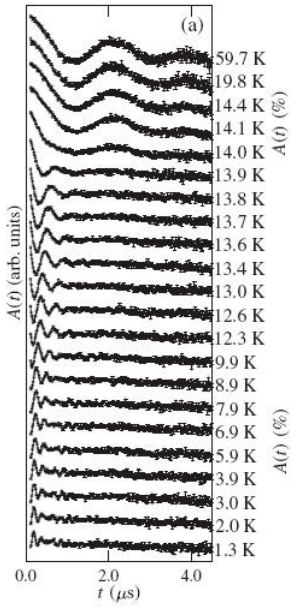

Figure 4.3: Muon spin resonance measurement[3]

The data in Figure 4.3 describes the change in the time dependence of the muon polarization as a function of temperature. At and below the critical temperature, a change in the oscillation is observed which is direct evidence of the muon's response to the local magnetic field at its interstitial stopping site within the sample. Below the critical temperature, higher frequency oscillations are observed. With maximum entropy analysis (distribution of probability with respect to entropy) of these oscillations, two nonequivalent muon stopping sites were identified for the Cs_2AgF_4 lattice.

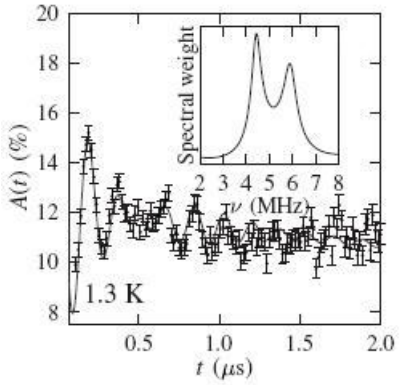

Figure 4.4: Graphical interpretation of the non-equivalency of the muon stopping sites[3]

The non-equivalency in the muon stopping sites can be measured by the muon decay signal. Data analysis has resulted in the conclusion that there is one muon stopping site in the [CsF] plane and one in the [AgF_2] plane of the Cs_2AgF_4 sample. This may be seen pictorially in Figure 4.5

From this experiment, the ferromagnetic nature of Cs_2AgF_4 found by McLain *et. al.*[9] was verified along with its critical temperature at 13.95 K. Since these measurements agree with those already reported in the literature,[9] the experimental details and writeup were submitted to *Physical Review B* and published as a rapid communication.[3] In response to the publication, theoreticians interested in Cs_2AgF_4 published results[48,49] which confirm the origin of

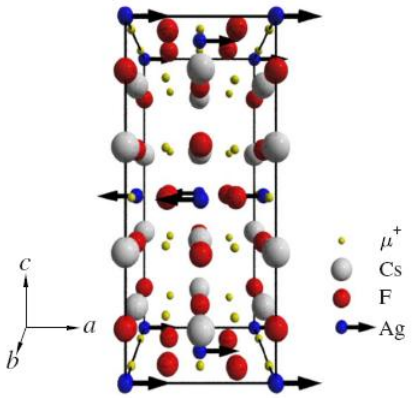

Figure 4.5: Muon stopping sites within the Cs_2AgF_4 lattice[3]

ferromagnetism in Cs_2AgF_4. The ferromagnetism is caused by a super exchange which occurs in the Ag−F−Ag bridges. This occurs through the staggered ordering of the $d_{z^2-y^2}$ and $d_{z^2-x^2}$ orbitals of the silver atoms.

4.2 Discussion of the structure measurements of the doped phases

In addition to the magnetic measurements discussed above, structural measurements of two of the doped derivatives of Cs_2AgF_4 were also recorded and analyzed. Sealed samples of $Cs_{1.9}Ba_{0.1}AgF_4$ and $Cs_{1.8}Ba_{0.2}AgF_4$ were measured on the X14A instrument at Brookhaven National Laboratory and the patterns analyzed using the GSAS program.[46]

Figure 4.6 through Figure 4.9 display the full X-ray powder diffraction pattern collected for the $Cs_{1.9}Ba_{0.1}AgF_4$ sample on the X14A instrument from $5.95 - 59.5$ 2θ, followed by magnification of important parts of the powder pattern collected at NSLS.

In these figures, the tick marks along the bottom of the pattern represent the phases present in the sample. The black tick marks represent the parent phase Cs_2AgF_4, the red

tick marks represent the starting material BaF_2, the blue tick marks represent the starting material AgF_2 and the green tick marks represent the starting material CsF. Since the doped phase $Cs_{1.9}Ba_{0.1}AgF_4$ is an uncharacteristic phase (there is not crystallographic information for this phase published in the literature), refinements were carried out based on the new phase's similarity to the parent compound Cs_2AgF_4. The barium atom was inputted into the lattice with the same crystallographic coordinates as the cesium atoms reported in the crystallographic information file for Cs_2AgF_4. Not surprisingly, additional peaks are observed in the pattern that do not match up with those of the parent compound or any of the starting materials. These indicate either the presence of a new phase or an impurity phase which was not considered during refinements.

Due to the inherent nature of a powder sample, which is composed of many crystallites instead of a single crystal, the presence of phases other than that of the bulk is assumed. Once the final refinements were finished, using the parent compound Cs_2AgF_4 as the model crystallographic system, each starting material was considered as a phase impurity. The colored tick marks in the images represent the X-ray powder pattern of each starting material. The amounts of these materials present in the sample are quite small, and the specific total phase fractions for the measured $Cs_{1.9}Ba_{0.1}AgF_4$ sample are given in Table 4.1.

Although the three starting materials are present, the fractions are so small that these materials should not be a source of considerable interfere with powder pattern analysis, although will most likly pose local structural and electronic effects at the atomic level. Once refinements produced close structure fits, keeping in mind that the phase under study will not have an identical structure to the parent material or any of the starting materials, a simulated crystal structure was produced using the DrawXTL software available free on the internet. The simulated crystal structure is displayed in Figure 4.10. Silver atoms are blue, fluorine

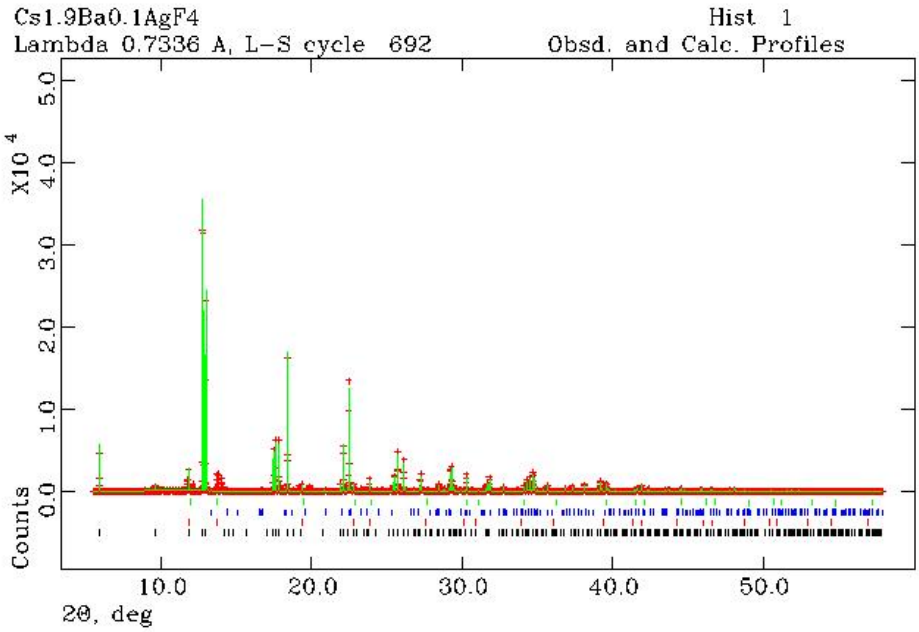

Figure 4.6: Powder diffraction pattern of $Cs_{1.9}Ba_{0.1}AgF_4$

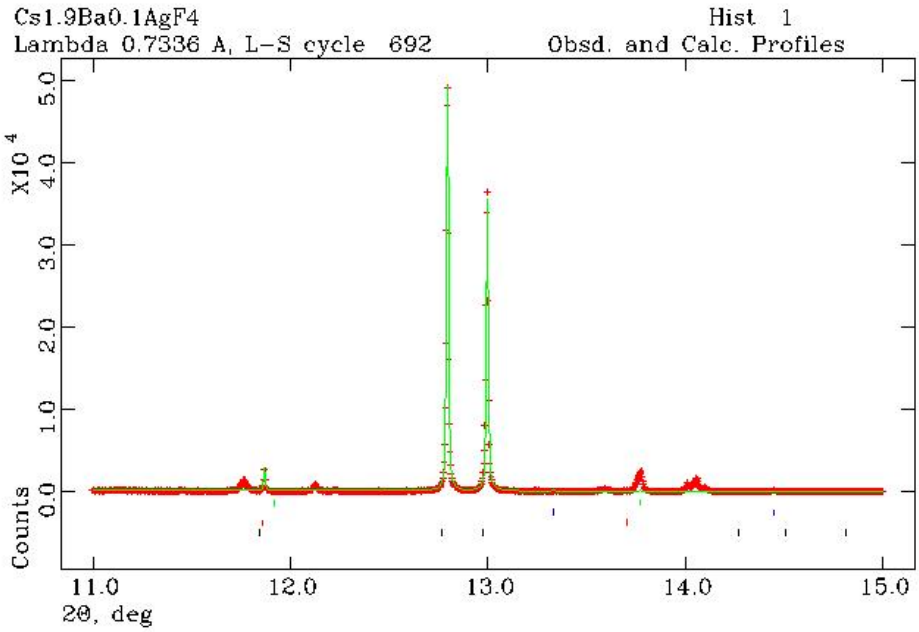

Figure 4.7: Powder diffraction pattern of $Cs_{1.9}Ba_{0.1}AgF_4$ from 11-15 degrees 2θ

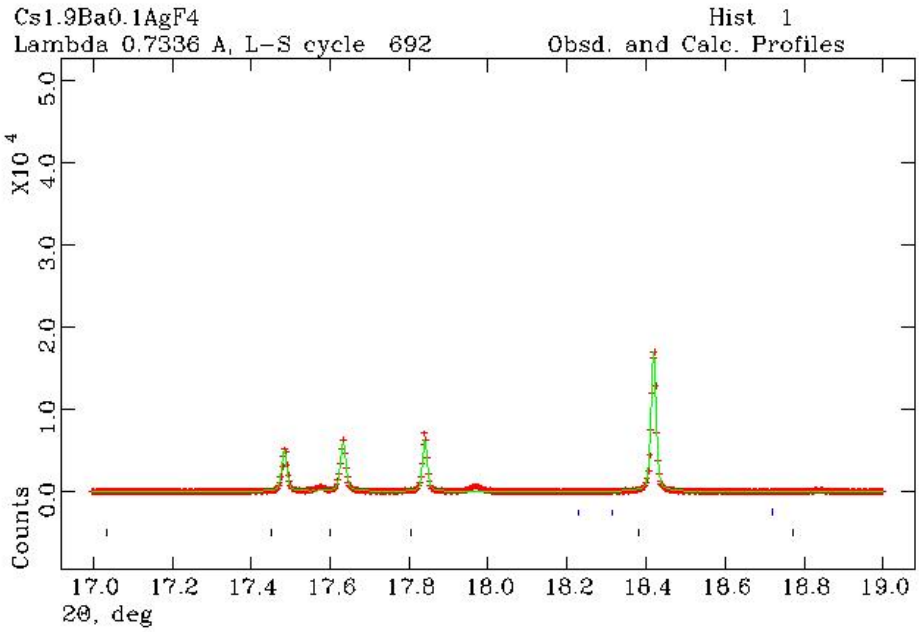

Figure 4.8: Powder diffraction pattern of $Cs_{1.9}Ba_{0.1}AgF_4$ from 17-19 degrees 2θ

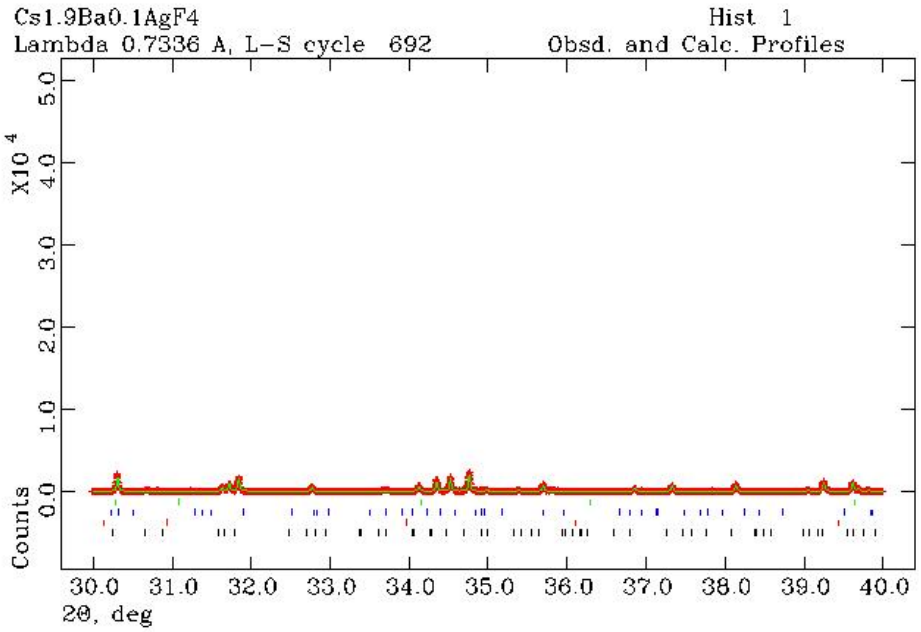

Figure 4.9: Powder diffraction pattern of $Cs_{1.9}Ba_{0.1}AgF_4$ from 30-40 degrees 2θ

Table 4.1: Phase fractions for $Cs_{1.9}Ba_{0.1}AgF_4$ sample

Phase	Phase fraction
Cs_2AgF_4	0.82293
BaF_2	$0.1x10^{-3}$
AgF_2	$0.81x10^{-3}$
CsF	$0.17x10^{-2}$

atoms are green and the cesium/barium is split with yellow representing the cesium fraction and red representing that of the barium.

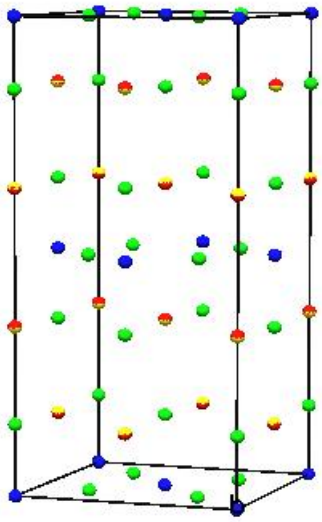

Figure 4.10: Simulated crystal structure of $Cs_{1.9}Ba_{0.1}AgF_4$ using DrawXTL software

Table 4.2 displays the unit cell parameters which have been found for the doped sample using the GSAS program, along with a comparison between these new parameters and those known for Cs_2AgF_4. The slight increase in the unit cell lengths of the doped sample in comparison to that of the parent phase, specifically along the a and b directions, suggest the

presence of mixed phases in the powder sample which are interfering with the ideal unit cell. Additionally, as the barium atoms are introduced to the sample, the Ag^{II} will begin to reduce to Ag^{I}, which leads to the conclusion that mixed valent silver fluorides will undoubtedly exist in these doped phases. Considering only the contribution of ionic radii and no magnetic effects, the replacement of the Cs^{+} ion with the smaller Ba^{2+} ion should decrease the size of the lattice. For comparison, the radius of a Cs^{+} ion is 1.69 Å and that of Ba^{2+} is 0.2 Å.[50] However, the increase in the unit cell does not follow the ionic radii suggestion, implying that there is more occurring at the atomic level than simple atom-atom interactions. Electronic interactions, specifically atom repulsion, may cause this increase in the unit cell and this effect may be more pronounced with the presence of interfering phases.

Table 4.2: Unit cell parameters for $Cs_{1.9}Ba_{0.1}AgF_4$ in comparison to Cs_2AgF_4

	$Cs_{1.9}Ba_{0.1}AgF_4$	Cs_2AgF_4
a	6.493965	4.58
b	6.494545	4.58
c	14.219487	14.192
α	90	90
β	90	90
γ	90	90

A second doped phase, $Cs_{1.8}Ba_{0.2}AgF_4$, was also prepared and measured using powder X-ray diffraction. The collected data is presented in the following figures. When comparing the two powder patterns collected, those of $Cs_{1.9}Ba_{0.1}AgF_4$ and $Cs_{1.8}Ba_{0.2}AgF_4$, there is a noticeable increase in the intensity of the unidentified phases which were noted in the

$Cs_{1.9}Ba_{0.1}AgF_4$ sample. In addition, the quality of the fit in the $Cs_{1.8}Ba_{0.2}AgF_4$ sample powder pattern is quite poor in comparison with that of the $Cs_{1.9}Ba_{0.1}AgF_4$ sample. This analysis suggests that with increased doping, the structure of the system begins to break down and produce a higher percent of secondary phases.

In the powder pattern figures, the black tick marks below the pattern represent the parent phase Cs_2AgF_4, the red tick marks represent the starting material BaF_2, the blue tick marks represent the starting material AgF_2 and the green tick marks represent the starting material CsF. These are the same labels as the $Cs_{1.9}Ba_{0.1}AgF_4$ sample for easy comparison of the overall appearance of the two collected powder patterns and a direct comparison between the peak intensities of all unidentified phases present.

In a similar manner, the fractions of these phases within the bulk material was analyzed and is displayed in the table directly following the powder diffraction data. The presence of alternate phases, although small, may have slight local structural consequences. In this case, as with the previously discussed doped sample, the unit cell is larger than that of the parent unit cell despite the substitution of a Cs^+ ion for the smaller Ba^{2+} ion.

Table 4.3: Phase fractions for $Cs_{1.8}Ba_{0.2}AgF_4$ sample

Phase	Phase fraction
Cs_2AgF_4	0.40116
BaF_2	$0.1x10^{-2}$
AgF_2	$0.33x10^{-3}$
CsF	$0.16x10^{-2}$

It becomes apparent, after comparing the alternate phases in both of the samples studied

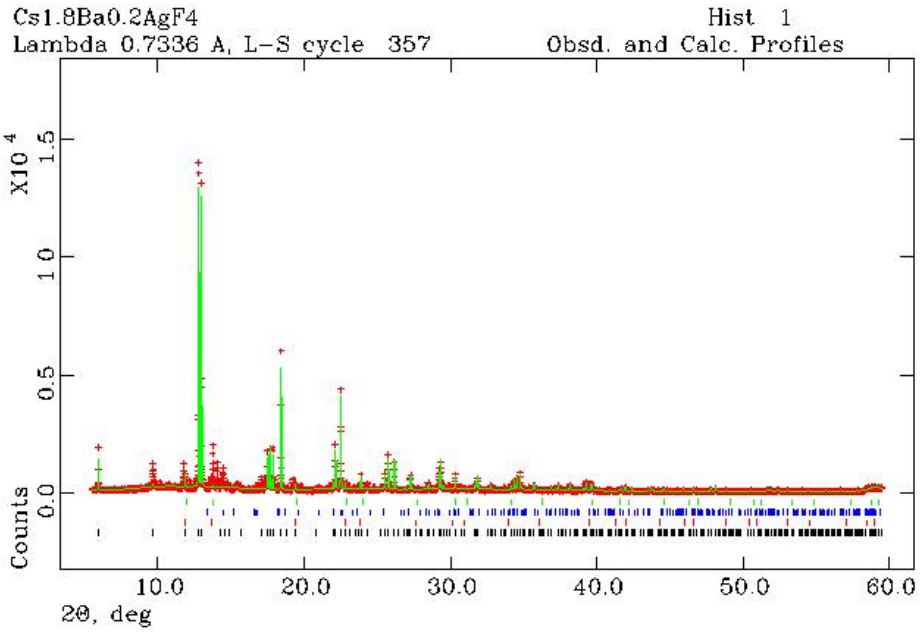

Figure 4.11: Powder diffraction pattern of $Cs_{1.8}Ba_{0.2}AgF_4$

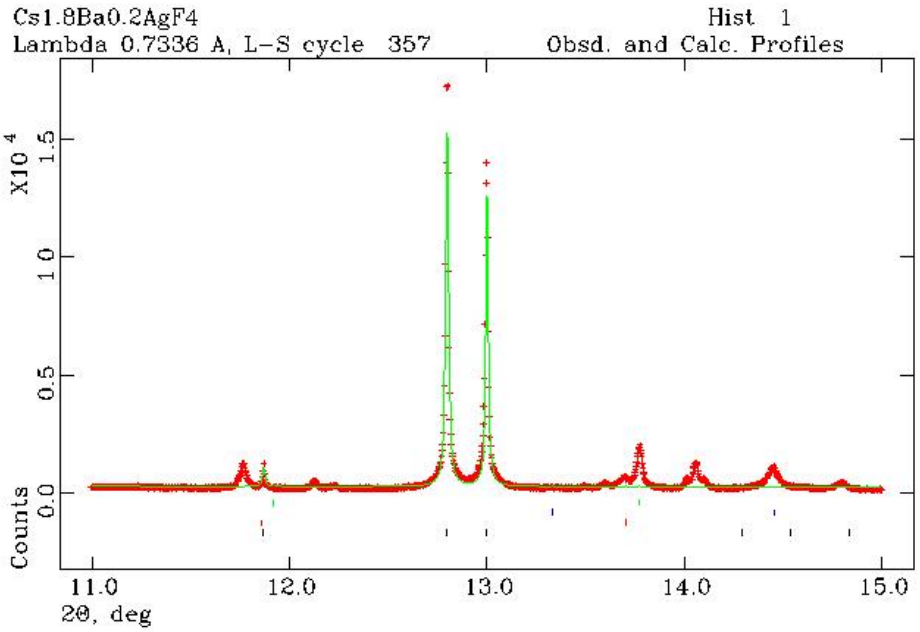

Figure 4.12: Powder diffraction pattern of $Cs_{1.8}Ba_{0.2}AgF_4$ from 11-15 degrees 2θ

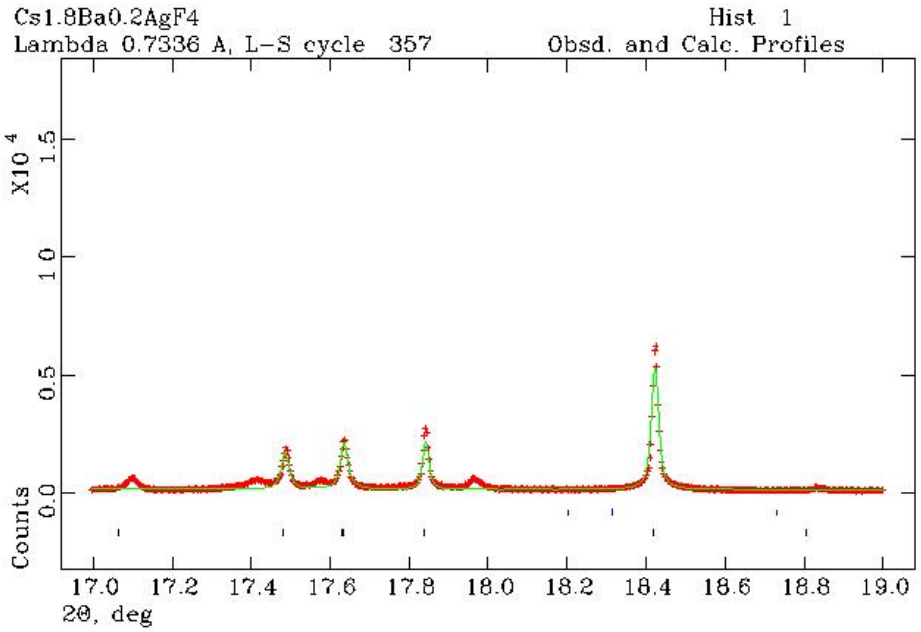

Figure 4.13: Powder diffraction pattern of $Cs_{1.8}Ba_{0.2}AgF_4$ from 17-19 degrees 2θ

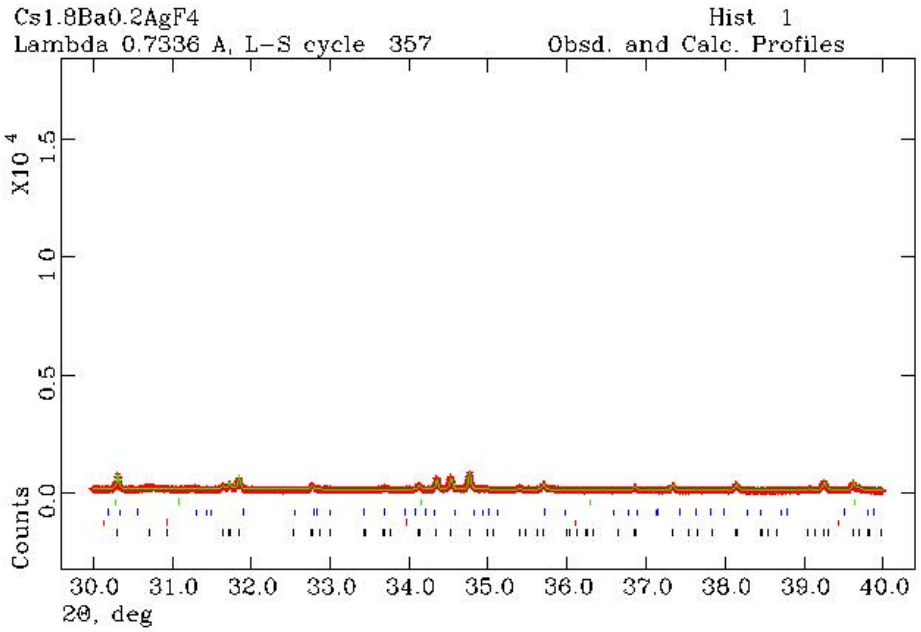

Figure 4.14: Powder diffraction pattern of $Cs_{1.8}Ba_{0.2}AgF_4$ from 30-40 degrees 2θ

by powder X-ray diffraction, that the doped silver fluoride phases of interest are not only challenging to synthesize, but also difficult to completely characterize. Interfering phases may change and alter the crystal structure of the bulk phases in such a way that the structural characteristics of the pure doped phases are masked. The figure below displays the simulated crystal structure for $Cs_{1.8}Ba_{0.2}AgF_4$ using DrawXTL.

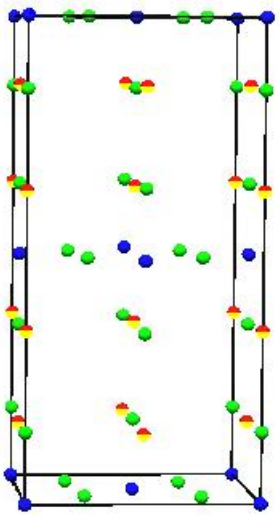

Figure 4.15: Simulated crystal structure of $Cs_{1.8}Ba_{0.2}AgF_4$ using DrawXTL software

In the figure, the silver atoms are blue, the fluorine atoms are green and the mixed occupancy cesium/barium sites are red/yellow (respectively). Additionally, the following table gives the unit cell parameters generated using GSAS, along with those reported for the parent compound Cs_2AgF_4. As can be seen, the unit cell volume of the doped compound $Cs_{1.8}Ba_{0.2}AgF_4$ is larger than that of the parent Cs_2AgF_4 compound.

As with the previously discussed sample, the unit cell lattice parameters for the bulk phase is slightly larger than that of the parent Cs_2AgF_4 phase. This is contrary to what would be expected when only considering the ionic radii of the Ba^{2+} ion which replaces the Cs^+ with doping. For final comparison, Table 4.5 shows the lattice parameters of the doped samples.

Table 4.4: Unit cell parameters for $Cs_{1.8}Ba_{0.2}AgF_4$ in comparison to Cs_2AgF_4

	$Cs_{1.8}Ba_{0.2}AgF_4$	Cs_2AgF_4
a	6.482013	4.58
b	6.483204	4.58
c	14.19519	14.192
α	90	90
β	90	90
γ	90	90

Table 4.5: Comparison of the lattice parameters of the doped samples

	$Cs_{1.9}Ba_{0.1}AgF_4$	$Cs_{1.8}Ba_{0.2}AgF_4$
a	6.493965	6.482013
b	6.494545	6.483204
c	14.219487	14.195198
α	90	90
β	90	90
γ	90	90

Despite the chemical treatment of the parent compound, chemical doping with Ba^{2+} ions, and preliminary structural data, the samples synthesized show no evidence of a superconducting phase. The hopeful existence of a superconducting phase was first measured by Dolgos *et. al.* (unpublished results), but the studies prove that the result of chemical doping is a change in the critical temperature, not the magnetochemistry of the system.

Chapter 5

Conclusions and future investigations

The data and discussion presented in this work merely scratches the surface of the overall potential of great scientific discovery with the ternary silver fluoride Cs_2AgF_4 and other silver fluoride phases. The ideal experiment would be to prepare polycrystalline samples (or more ideally, single crystal samples) of the parent compound Cs_2AgF_4 as well as the doped phases, $Cs_{1.9}Ba_{0.1}AgF_4$ and $Cs_{1.8}Ba_{0.2}AgF_4$, in large enough quantity to send an appreciable amount for variable temperature powder X-ray diffraction, neutron scattering, muon spin resonance and SQUID experiments in one large facility visit. With data from these experiments on the same batch of sample, an accurate overall analysis can be made on these phases in order that their properties may be characterized.

A final set of data, which was collected during this project but not yet analyzed or fully refined, is presented in Figures 5.1- 5.2. This data provides just a glimpse of the types of changes which would take place if the doping scheme was to be carried out further. At some point, the structure of the doped systems would undoubtedly begin to break down, but synthetic investigations to find out exactly what that point is would provide more structural and magnetochemical information on this system.

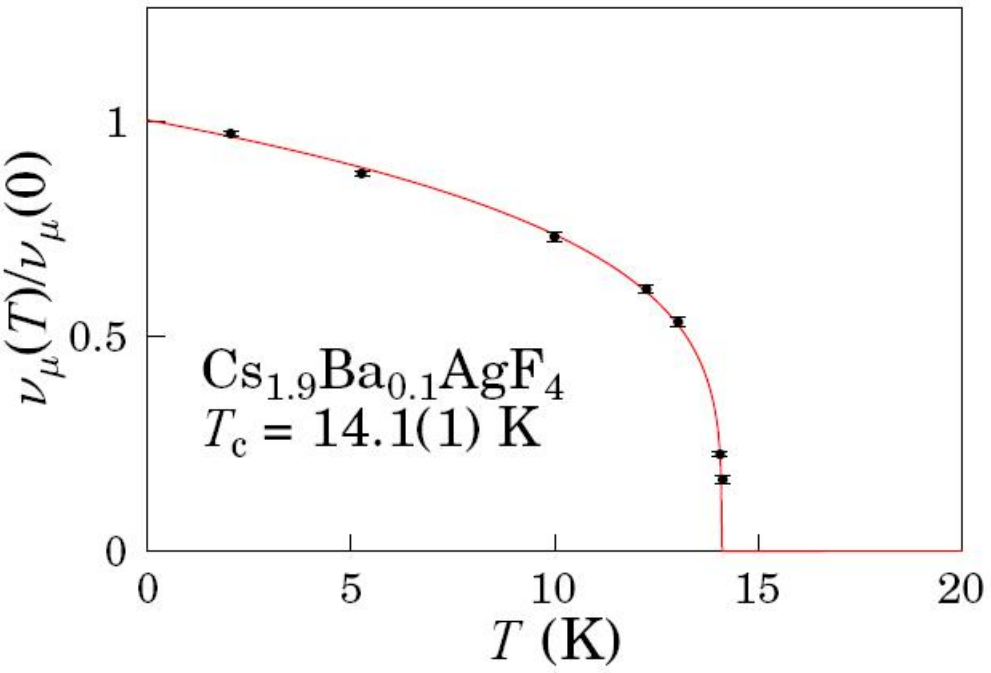

Figure 5.1: Muon spin resonance data for $Cs_{1.9}Ba_{0.1}AgF_4$ collected at PSI

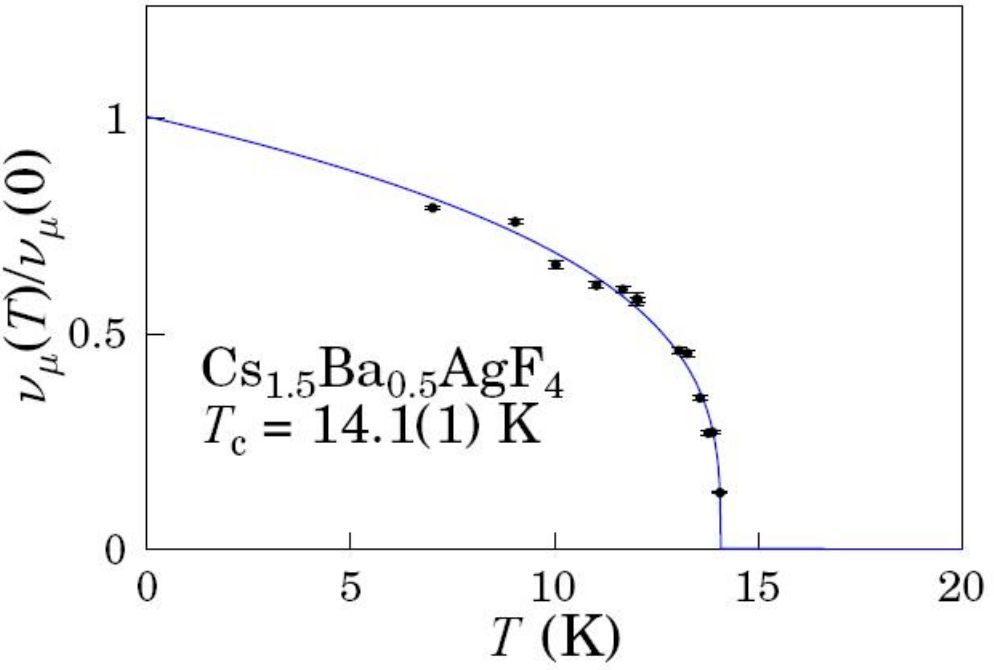

Figure 5.2: Muon spin resonance data for $Cs_{1.5}Ba_{0.5}AgF_4$ collected at PSI

The data presented is a comparison of critical temperatures of $Cs_{2-x}Ba_xAgF_4$ with x=$0.1, 0.5$ which were determined by muon spin resonance at PSI in Switzerland. Data was collected for samples with x=$0.1, 0.2, 0.3, 0.4$ and 0.5, with only the smallest and largest doping amounts displayed. According to this data (and the data from samples of intermediate composition to those presented), the critical temperature does not change with higher dopant levels. While this is an interesting result, the data may also represent an alternate scenario, in which no matter how much dopant is added, the same phase is formed with a higher percentage of unreacted starting material when a higher dopant level is used. However, this data is in direct contrast with neutron scattering data recorded (unreported) by a group member on $Cs_{1.9}Ba_{0.1}AgF_4$, which suggests a large increase in critical temperature with minimal doping.

Despite preliminary data on the further doped silver fluorides, in comparison with the copper oxide analogues, the ideal doping is just enough to promote the onset of orbital alignment to produce a superconducting phase. Those noted for the copper oxides which have been characterized are only at dopant levels with x=0.2 for the doping scheme $La_{2-x}Ba_xCuO_4$.[5] Due to the structural similarity of these species to known superconductors, they present a promising deviation from what is already known in order to discover something truly revolutionary. Even during the time of writing of this work, a group led by Grochala[51] has altered the study of possible superconductivity in silver fluorides in another direction. Due to the overwhelming evidence for the antiferromagnetism in La_2CuO_4 playing a role in the superconductivity of its doped derivatives, Grochala has proposed ways in which to synthetically prepare an antiferromagnetic Ag^{II} species. An antiferromagnetic Ag^{II} species would not only mimic the known superconductors with the presence of a Jahn-Teller distorted octahedra, which is an important feature for superconductivity in these systems, but it would also replicate the antiferromagnetism seen in the doped copper oxide phases.

The copper oxides present a more applicable system for superconductivity for everyday use due to their air stability. The race for a room temperature superconductor ensues for now, with an ever present hope of unveiling the intricate mechanism by which the phenomena occurs.

Experimental

Synthesis of $Cs_{(2-x)}Ba_xAgF_4$

All synthetic procedures were carried out in an argon filled glove box with the residual H_2O and O_2 levels below 0.1ppm. The starting materials were purchased from Strem Chemicals Inc.© (2009).[†]

For each synthesis, silver (II) fluoride (AgF_2) was weighed out in an aluminum weigh boat and ground to a fine powder using an agate mortar and pestle. Next, the cesium fluoride (CsF) was weighed and added to the AgF_2 in the mortar and pestle. The two solids were ground together until a homogeneous powder was reached (assessment by sight). Finally, the barium fluoride (BaF_2) was weighed and added to the solid mixture (where necessary) and all of the starting materials were ground together into a fine powder mixture.

Once ground sufficiently, the solid mixture was transferred to a platinum crucible. This was placed into a sand filled heating mantle, equipped with a thermocouple to measure temperature. The reaction was heated to 320 °C for 24 h. The reaction was then cooled, re-ground and heated for an additional 12 hours at 320 °C. All products were ground upon final cooling and stored in plastic screw top vials until analyzed.

Table 5.1 provides the weights of starting materials used for *all* phase syntheses. Only

[†]Strem Chemicals Inc., 7 Mulliken Way, Newburyport, MA, 01950, USA, www.strem.com

certain phases were analyzed by diffraction and MuSR.

Table 5.1: Quantities of starting materials (in moles) used in synthesis of $Cs_{(2-x)}Ba_xAgF_4$ phases

x	AgF_2 (mol)	CsF (mol)	BaF_2 (mol)
0	0.0077	0.015	0
0.05	0.03	0.0067	0.0017
0.1	0.002	0.004	0.00022
0.15	0.003	0.00634	0.0005
0.2	0.002	0.0039	0.00044
0.25	0.003	0.0059	0.00086
0.3	0.003	0.0058	0.001
0.4	0.003	0.005	0.001
0.5	0.003	0.005	0.0017
0.6	0.003	0.0047	0.002

For the powder X-ray diffraction experiments, a small sample of phase ($Cs_{1.9}Ba_{0.1}AgF_4$ and $Cs_{1.8}Ba_{0.2}AgF_4$) were each placed into a 0.3mm diameter quartz capillary tube (Charles Supper Company, Inc)[†]. These were flame sealed and transported directly to NSLS for diffraction experiments.

For the muon spin resonance experiment, a sample of Cs_2AgF_4 was sealed in a gold plated titanium sample holder equipped with a gold o-ring. This sample was shipped directly to ISIS for the MuSR experiment.

[†]Carles Supper Company, In., 15 Tech Circle, Natick, MA, 01769, USA, www.charles-supper.com

Bibliography

[1] W. Grochala and R. Hoffman, "Real and hypothetical intermediate-valence Ag^{II}/Ag^{III} and Ag^{II}/Ag^{I} fluoride systems as potential superconductors," *Angew. Chem. Int. Ed.*, vol. 40, pp. 2742–2781, 2001.

[2] W. Grochala, "Small changes, big consequences," *Nature Materials*, vol. 5, pp. 513–514, 2006.

[3] T. Lancaster, S. J. Blundell, P. J. Baker, W. Hayes, S. R. Giblin, S. E. McLain, F. L. Pratt, Z. Salman, E. A. Jacobs, J. F. C. Turner, and T. Barnes, "Intrinsic magnetic order in Cs_2AgF_4 detected by muon-spin relaxation," *Physical Review B*, vol. 75, pp. 220408–1 – 220408–4, 2007.

[4] K. Banynard, "Diamagnetism as a test of wave functions for some simple molecules," *The Journal of Chemical Physics*, vol. 33, no. 3, pp. 832–836, 1960.

[5] J. Jorgensen, H.-B. Schuttler, D. Hinks, I. D.W. Capone, K. Zhang, M. Brodsky, and D. Scalapino, "Lattice instability and high-t_c superconductivity in $La_{2-x}Ba_xCuO_4$," *Physical Review Letters*, 1987.

[6] R. Cava, R. van Dover, B. Batlogg, and E. Rietman, "Bulk superconductivity at 36k in $La_{1.8}Sr_{0.2}CuO_4$," *Physical Review Letters*, 1987.

[7] T. Takami, J. Zhou, J. Cheng, J. Goodenough, K. Matsubayashi, and Y. Uwatoko, "Study of the onset of superconductivity in underdoped $La_{2-x}Sr_xCuO_4$," *New Journal of Physics*, 2009.

[8] M. Khan, Y. Miro, I. Tanaka, and H. Kojima, "Growth and superconductivity of $La_{2-x}Ca_xCuO_4$ single crystals," *Physica C*, 1996.

[9] S. E. McLain, M. R. Dolgos, D. A. Tennant, J. F. C. Turner, T. Barnes, T. Proffen, B. C. Sales, and R. I. Bewley, "Magnetic behaviour of layered Ag^{II} fluorides," *Nature Materials*, vol. 5, pp. 561–566, 2006.

[10] C. Kritayakomupong, "The jahn-teller effect of the Ag^{II} ion in aqueous solution: A hybrid *ab initio* quantum mechanical/molecular mechanical molecular dynamics simulation," *Chemical Physics Letters*, vol. 455, pp. 207–212, 2008.

[11] N. Bartlett, G. Lucier, C. Shen, W. C. J. an dL. Chacon, J. Munzenberg, and B. Zemva, "The oxidizing properties of cationic high oxidation state transition-element fluoro species," *Journal of Fluorine Chemistry*, vol. 71, pp. 163–164, 1995.

[12] B. Zemva, R. Hagiwara, W. J. C. Jr., K. Lutar, A. Jesih, and N. Bartlett, "Spontaneous oxidation of xenon to Xe(II) by cationic Ag(II) in anhydrous hydrogen fluoride solutions," *Journal of the American Chemical Society*, vol. 112, pp. 4846–4849, 1990.

[13] B. Standke and M. Jansen, "Preparation and crystal structure of Ag_2O_3," *Z. Anorg. allg. Chem.*, pp. 39–46, 1986.

[14] W. S. Graff and H. H. Stadelmaier, "Higher oxides of silver," *Journal of the Electrochemical Society*, pp. 446–449, 1958.

[15] M. Jansen and P. Fischer, "Eine neue darstellungsmethode fur monoklines silver (I_1II)oxid (AgO), einkristallzuchtung und rontgenstrukturanalyse," *Journal of the Less-Common Metals*, pp. 123–131, 1987.

[16] J. McMillan, "Magnetic properties and crystalline structure of AgO," *Journal of Inorganic Nuclear Chemistry*, 1959.

[17] H. Jahn and E. Teller, "Stablilty of polyatomic molecules in degenerate electronic states. i. orbital degeneracy," *Proceedings of the Royal Society of London A*, pp. 220–235, 1937.

[18] D.-Y. Liu, F. Lu, and L.-J. Zou, "Anharmonic effect on lattice distortion, orbital ordering and magnetic properties in Cs_2AgF_4," *Journal of Physics: Condensed Matter*, vol. 21, pp. 026014–1 – 026014–6, 2009.

[19] L. Jennings and C. Sewnson, "Effects of pressure on the superconducting transition temperatures of SnInTaTl and Hg," *Physical Review*, vol. 112, no. 1, pp. 31–43, 1952.

[20] P. Entel, M. Crisan, G. Bongi, and W. Klose, "Possible coexistence of superconductivity and magnetism in layered compounds," *Journal of Low Temperature Physics*, vol. 23, pp. 157–176, 1976.

[21] R. Cava, R. van Dover, B. Batlogg, and E. Rietman, "Bulk superconductivity at 36k in $La_{1.8}Sr_{0.2}CuO_4$," *Physical Review Letters*, vol. 58, no. 4, pp. 408–410, 1987.

[22] C. Rao, P. Ganguly, A. Raychaudhuri, R. M. Ram, and K. Sreedhar, "Identification of the phase responsible for high-temperature superconductivity in $Y-Ba-Cu$ oxides," *Nature*, vol. 326, pp. 856–857, 1987.

[23] P. Dai, B.C.Chakoumakos, G. Sun, K. Wong, Y. Xin, and D. Lu, "Synthesis and neutron powder diffraction study of the superconductor $HgBa_2Ca_2Cu_3O_8-d$ by tl substitution," *Physics C*, pp. 201–206, 1995.

[24] J. Bardeen, L. Cooper, and J. Schrieffer, "Theory of superconductivity," *Physical Review*, vol. 108, no. 5, pp. 1176–1204, 1957.

[25] R. Allen, G. Alldredge, and R. de Wette, "Lattice vibrations and superconductivity in layered structures," *Physical Review B*, vol. 2, no. 7, pp. 2570–2573, 1970.

[26] J. Bednorz and K. Muller, "Possible high T_c superconductivity in the Ba−La−Cu−O system," *Zeitschrift fur Physik B, Condensed Matter*, vol. 64, pp. 189–193, 1986.

[27] C. Politis, J. Geerk, M. Dietrich, and B. Obst, "Superconductivity at 40 k in $La_{1.8}Sr_{0.2}CuO_4$," *Zeitschrift fur Physik B, Condensed Matter*, vol. 66, pp. 141–146, 1987.

[28] M. Wilhelm and O. Eibl, "Preparation and properties of superconducting (T_c= 114K) Pb-doped Bi−Sr−Ca−Cu oxide," *Solid State Communications*, vol. 70, no. 2, pp. 137–140, 1989.

[29] W. Grochala, "On similarities and differences of the electronic structure for $Cu(II)_/O^{2-}$ and $Ag(II)_/F^-$ infinite layer compounds," *Scripta Materialia*, vol. 55, pp. 811–814, 2006.

[30] B. Zemva, K. Lutar, A. Jesih, W. J. Casteel, A. P. W. Jr., D. E. Cox, R. B. V. Dreele, H. Borrmann, and N. Bartlett, "Silver trifluoride: Preparation, crystal structure, some properties and comparison with AuF_3," *Journal of the American Chemical Society*, vol. 113, pp. 4192–4198, 1990.

[31] C. Shen, B. Zemva, G. M. Lucier, O. Graudjus, J. A. Allman, and N. Bartlett, "Disproportionation of Ag(II) to Ag(I) and Ag(III) in fluoride systems and syntheses and structures of $(AgF^+)_2AgF_4^-MF_6^-$ salts (M= As, Sb, Pt, Au, Ru)," *Inorganic Chemistry*, vol. 38, pp. 4570–4577, 1999.

[32] G. Lucier, J. Whalen, and N. Bartlett, "High yield room temperature syntheses of $KAgF_4$ and AgF_3 and the preparation and unit cell of ceLiAgF4," *Journal of Fluorine Chemistry*, vol. 89, pp. 101–104, 1998.

[33] G. Lucier, C. Shen, W. Casteel, L. Chacon, and N. Bartlett, "Some chemistry of high oxidation state transition metal fluorides in anhydrous HF," *Journal of Fluorine Chemistry*, vol. 72, pp. 157–163, 1995.

[34] R. Fischer and B. Muller, "Crystal structure of Ag(II)F[Ag(III)F_4]," *Zeitschrift fuer Anorganische und Allgemeine Chemie*, vol. 628, pp. 2592–2596, 2002.

[35] B. Muller, "Structure of quaternary fluorides iwth divalent silver: M(I)Ag(II)M(III)F_6 with M(I)= rubidium or cesium and M(III)= aluminum, gallium or iron," *Journal of Fluorine Chemistry*, vol. 17, pp. 317–329, 1981.

[36] B. Muller, "New complex fluorides with silver (2+) and palladium (2+): NaM(II)Zr_2F_{11} M(II)= Ag, Pd and silver palladium zirconium fluoride ($AgPdZr_2F_{11}$)," *Zeitschrift fuer Anorganische und Allgemeine Chemie*, vol. 553, pp. 205–211, 1987.

[37] B. Muller, "High pressure modifications of palladium difluoride and silver difluoride," *Naturwissenschaften*, vol. 66, pp. 519–520, 1979.

[38] B. Muller, "New ternary silver (II) fluorides: $Ag(II)_3M(IV)_2F_{14}$ (M(IV)= zirconium,

hafnium)," *Zeitschrift fuer Anorganische und Allgemeine Chemie*, vol. 553, pp. 196–204, 1987.

[39] O. Graudejus and B. Muller, "Ag^{2+} in trigonal bipyrimidal surrounding: New fluorides with divalent silver $AgM(II)_3M(IV)_3F_{20}$," *Zeitschrift fuer Anorganische und Allgemeine Chemie*, vol. 622, pp. 1549–1556, 1996.

[40] A. Jesih, K. Lutar, B. Zemva, B. Bachmann, B. Muller, and R. Hoppe, "Single crystal investigations on AgF_2," *Zeitschrift fuer Anorganische und Allgemeine Chemie*, vol. 588, pp. 77–83, 1990.

[41] R. Eujen and B. Zemva, "NMR spectra of AgF_4^-," *Journal of Fluorine Chemistry*, vol. 99, pp. 139–140, 1999.

[42] A. Goryunkov, V. Markov, O. Boltalina, B. Zemva, A. Abdul-Sada, and R. Taylor, "Reaction of silver(I) and silver(III) with C_{60}: thermodynamic control over fluorination level," *Journal of Fluorine Chemistry*, vol. 112, pp. 191–196, 2001.

[43] T. Nakajima, Y. Matsuo, B. Zemva, and A. Jesih, "Synthesis of fluorine-graphite intercalation compounds by elemental fluorine and high oxidation-state transition-metal fluorides," *Carbon*, vol. 23, pp. 1595–1598, 1986.

[44] D. Noakes, E. Ansaldo, and G. Luke, "Muon spin relaxation study of the $(F-\mu-F)$-ion in magnetic fluorides," *Journal of Applied Physics*, vol. 73, no. 10, pp. 5666–5668, 1993.

[45] R. Stolveik, "Prediction of entropy of vaporization based on correlation with the normal boiling point," *Acta Chemica Scandinavica*, vol. 43, pp. 860–867, 1989.

[46] A. Larson and R. V. Dreele, "General structure analysis system (gsas)," *Los Alamos National Laboratory Report LAUR-86-748*, 2000.

[47] L. McCusker, R. V. Dreele, D. Cox, D. Louer, and P.Scardi, "Rietveld refinement guidelines," *Journal of Applied Crystallography*, pp. 36–50, 1999.

[48] X. Hao, Y. Xu, Z. Wu, D. Zhou, X. Liu, and J. Meng, "Orbital ordering in Cs_2AgF_4 from first principles," *Physical Review B*, vol. 76, pp. 054426–1 – 054426–6, 2007.

[49] H. Wu and D. I. Khomskii, "Orbital ordering in the ferromagnetic insulator Cs_2AgF_4 from first principles," *Physical Review B*, vol. 76, pp. 155115–1 – 0155115–4, 2007.

[50] L. Pauling, *General Chemistry*. 1970.

[51] Z. Mazej, E. Goreshnik, Z. Jaglicic, B. Gawel, W. Lasocha, D. Grzybowska, T. Jaron, D. Kurzydlowski, P. Malinowski, W. Kozminski, J. Szydlowska, P. Leszczynski, and W. Grochala, "$KAgF_3$, K_2AgF_4 and $K_3Ag_2F_7$, important steps towards a layered antiferromagnetic fluoroargentate (II)," *CrystEngComm*, pp. 1702–1710, 2009.